Nucl Eng Technol 47 (2015) 791–803

Available online at www.sciencedirect.com

ScienceDirect

journal homepage: http://www.journals.elsevier.com/nuclear-engineering-and-technology/

Original Article

POINTWISE CROSS-SECTION-BASED ON-THE-FLY RESONANCE INTERFERENCE TREATMENT WITH INTERMEDIATE RESONANCE APPROXIMATION

MEER BACHA * *and HAN GYU JOO*

Department of Nuclear Engineering, Seoul National University, 1 Gwanak-ro Gwanak-gu, Seoul 151-742, Republic of Korea

ARTICLE INFO

Article history:
Received 14 April 2015
Received in revised form
23 July 2015
Accepted 23 July 2015
Available online 9 October 2015

Keywords:
Dancoff factor
Enhanced neutron current method
Equivalence theory
Resonance integral
Self-shielding
Subgroup method

ABSTRACT

The effective cross sections (XSs) in the direct whole core calculation code nTRACER are evaluated by the equivalence theory-based resonance-integral-table method using the WIMS-based library as an alternative to the subgroup method. The background XSs, as well as the Dancoff correction factors, were evaluated by the enhanced neutron-current method. A method, with pointwise microscopic XSs on a union-lethargy grid, was used for the generation of resonance-interference factors (RIFs) for mixed resonant absorbers. This method was modified by the intermediate-resonance approximation by replacing the potential XSs for the non-absorbing moderator nuclides with the background XSs and neglecting the resonance-elastic scattering. The resonance-escape probability was implemented to incorporate the energy self-shielding effect in the spectrum. The XSs were improved using the proposed method as compared to the narrow resonance infinite mass-based method. The RIFs were improved by 1% in ^{235}U, 7% in ^{239}Pu, and >2% in ^{240}Pu. To account for thermal feedback, a new feature was incorporated with the interpolation of pre-generated RIFs at the multigroup level and the results compared with the conventional resonance-interference model. This method provided adequate results in terms of XSs and k-eff. The results were verified first by the comparison of RIFs with the exact RIFs, and then comparing the XSs with the McCARD calculations for the homogeneous configurations, with burned fuel containing a mixture of resonant nuclides at different burnups and temperatures. The RIFs and XSs for the mixture showed good agreement, which verified the accuracy of the RIF evaluation using the proposed method. The method was then verified by comparing the XSs for the virtual environment for reactor application-benchmark pin-cell problem, as well as the heterogeneous pin cell containing burned fuel with McCARD. The method works well for homogeneous, as well as heterogeneous configurations.

* *Corresponding author.*
E-mail address: meerbacha@yahoo.com (M. Bacha).

http://dx.doi.org/10.1016/j.net.2015.09.001
1738-5733/Copyright © 2015, Published by Elsevier Korea LLC on behalf of Korean Nuclear Society.

1. Introduction

The equivalence theory-based [1] resonance-integral (RI) method [2] is commonly used for self-shielding calculations in many lattice-physics codes. One of the most challenging tasks in self-shielding calculations is the generation of effective cross sections (XSs) in mixed-absorber configurations. Most methods, such as the subgroup method [3], are efficient and accurate in determining effective XSs for isolated resonant nuclides. In the case of mixed absorbers, these methods apply some adjustments or modifications to the XSs. There can be unknown weaknesses in such methods concerning mixed-absorber configurations.

The nTRACER direct whole-core calculation code [4], which is capable of dealing with the local heterogeneity of the core constituents without homogenization in the single-step calculation, employs the subgroup method for resonance treatment. It uses its own multigroup (MG) XS library generated from the ENDF-B/VII XS data [5] through an internal procedure that also determines the optimized subgroup parameters [3]. Recently, an alternative XS processing feature was introduced in nTRACER in order to utilize the WIMS-IAEA XS library. This library contains the RI data and no subgroup parameters. In this article, the in-house nTRACER library and the WIMS library [6] will be abbreviated as nTL and WIL, respectively. In the conventional RI-based resonance-treatment methods, the RI table is used to generate the effective XSs in a heterogeneous configuration and the RI data are tabulated as a function of background XSs and temperatures. The conventional RI method was implemented in nTRACER in conjunction with WIL, for which no subgroup data are available. For the determination of the background XSs under equivalence theory, the enhanced neutron-current method [7] was applied. This method directly evaluates the background XSs and does not need the escape XSs or the Dancoff factors.

The resonance treatment of an isolated resonant nuclide can be accurate in terms of effective XSs. With multiple resonant nuclides, the resonance interference among various resonance nuclides must be treated properly in order to accurately obtain the effective XSs. The most accurate method for evaluating the effective XSs in the mixed absorbers is to solve the neutron-slowing equation for all resonant nuclides in a mixture. This method is feasible at the pin-cell level, but is impractical for the assembly and core calculations using current computational resources. One of the approximations involves considering only one resonant nuclide at a time without considering the effects of other available resonant nuclides. This approximation would result in large discrepancies in XSs in the mixed-absorbers case. Another approximation is to augment the background XS with the average absorption XS of the system. This approach is known as the conventional Bondarenko iteration approach [3] for resonance interference treatment. In this approach, each resonant nuclide influences on all other nuclides in the mixture. The larger the absorption XS of the nuclide, the greater its impact on other resonant nuclides. In this approach, the effective XSs always increase because of the augmentation of absorption XSs to the background XSs. Therefore, the conventional method cannot show the decreasing trend of XSs from the interference. To account for the resonance interference in the mixture of resonance absorbers, some methods modify the resonance integrals by the density ratios [8]. However, the larger the number of absorbers in the mixture, the more complex the method. Recently, a new method was developed for the evaluation of resonance interference factors (RIFs) at the multigroup level [9]. This method generates the RIFs for the resonant nuclides at various temperatures, compositions, and background XSs. These tabulated multigroup factors can be interpolated for the temperature and background XSs. This method provides good results at the cost of high computational burden.

The term RIF was introduced in a much earlier paper [10] in which the microscopic XSs were tabulated on a union-lethargy interval for each resonant absorber and temperature. This method was based on the narrow resonance infinite mass (NRIM) or the wide-resonance (WR) flux approximations for on-the-fly generation of the RIFs. These calculations were performed once per burnup step for each composition and background XS. This method provided better results than the conventional method, however, did not adequately model the thermal feedback. A method is required to improve the accuracy of XSs, as well as present a better and more robust way of treating temperature feedback.

This study presents a modification of the above method. Instead of using the WR or NRIM approximation for the resonant absorbers, the intermediate resonance (IR) approximation was used with the neglect of the resonance elastic-scattering term. For the accuracy of XSs, the resonance-escape probability was implemented to account for the energy self-shielding effect in the spectrum. This study aimed to implement an efficient resonance-interference treatment model in nTRACER with WIL. With this method, the XSs in the resonance-energy range were accurately and robustly evaluated. The accuracy of the XSs increased using the proposed method and the thermal-feedback effect was handled with interpolation of temperature-dependent RIFs at the multigroup level, with pre-generated RIFs interpolated for the system temperature. This method was more accurate than both the conventional and NRIM-based methods and efficiently treated temperature feedback with no computational cost. The application of the resonance-escape probability increased the accuracy of RIFs, as well as XSs. In this manuscript, the IR-based XS table method will be denoted as XST, while the IR-based XS table method with resonance-escape probability will be expressed as modified XST. In this method, the RIF calculation was performed once per burnup step, with little extra computational burden and no large amounts of memory required. This study focuses on the applicability of this method to the homogeneous pin-cell problem at various burnups and temperatures, and the heterogeneous virtual environment for reactor application (VERA)-benchmark pin-cell problems. A heterogeneous pin cell with burned fuel is also analyzed and the reliability of the thermal-feedback effect for the RIFs is discussed in detail.

2. Materials and methods

The Bondarenko-iteration approach incorporates the interference effects of the resonant nuclides on the target nuclide in a mixture by making a modification to the background XSs with the absorption XSs. This approach cannot deal with the decreasing trend of XSs in some energy groups because the effective XSs increase with the background XSs. However, the XS table approach [10] employs the NRIM-flux approximation or WR approximation. This method will be referred to as the NRIM-based method. This method has high inaccuracy related to XSs. Moreover, it cannot handle the thermal-feedback effect on the RIFs. For a better flux calculation, a modification can be undertaken using the IR approximation and with the neglect of the resonance elastic-scattering source. The number of post-peak neutrons will be less than the number of pre-peak neutrons because some of the neutrons will be absorbed in the resonance peak. This effect is incorporated by the resonance-escape probability. In this new approach, the pointwise XSs, generated on a union grid for each resonant nuclide at various temperatures, are needed. This method using the resonance-escape probability is the modified XST. The method for the generation and tabulation of pointwise XSs is discussed in the following section. The method for on-the-fly determination of RIFs is also explained in detail.

2.1. *Pointwise XSs generation*

The unionized pointwise XSs for a resonant nuclide can be generated using the NJOY-BROADR module [11]. The procedure is as follows: (1) generate the pointwise absorption and fission XS files for each nuclide at several temperatures; (2) convert the pointwise XSs to union-grid XSs for all isotopes with a very narrow lethargy interval; (3) tabulate the XSs for each resonant nuclide, reaction, and temperature.

2.2. *Background XS calculation*

Before defining the RIFs, the background XS is discussed in detail in this section [2,6]. The effective XSs are evaluated by interpolating the RI data at a specific background XS and temperature of the system. The RIFs to be evaluated are also functions of the background XS and temperature. Therefore, background XS evaluation is important for all of the resonance calculations.

By definition, the background XS for a homogeneous system can be obtained by:

$$\sigma_b^{\mathrm{hom}} = \lambda^r \sigma_p^r + \sum_{\substack{i=1 \\ i \neq r}}^{N} \frac{N^i}{N^r} \lambda^i \sigma_p^i \tag{1}$$

where σ_b^{hom} is the background XS for the resonant nuclide r; σ_p^r, σ_p^i are the potential XSs for the resonant and non-resonant nuclides, respectively, and $\lambda's$ are the Goldstein-Cohen intermediate-resonance factors. N represents the total number of nuclides in the mixture, while N^i and N^r represent the number densities of the non-resonant and resonant nuclides, respectively.

For a heterogeneous isolated system, the background XS is augmented by the escape XS as follows:

$$\sigma_b^{het} = \sigma_b^{\mathrm{hom}} + \sigma_e \tag{2}$$

Substituting the background XS for homogeneous configuration in Eq. (2),

$$\sigma_b^{het} = \lambda^r \sigma_p^r + \sum_{\substack{i=1 \\ i \neq r}}^{N} \frac{N^i}{N^r} \lambda^i \sigma_p^i + \sigma_e \tag{3}$$

where $\sigma_e = \frac{\Sigma_e}{N^r}$ is the escape XS for resonance nuclide r.

To incorporate the shadowing effect of other fuel rods in the lattice, it is necessary to multiply the Dancoff factor (D) by the escape XS:

$$\sigma_b^{het} = \lambda^r \sigma_p^r + \sum_{\substack{i=1 \\ i \neq r}}^{N} \frac{N^i}{N^r} \lambda^i \sigma_p^i + D\sigma_e \tag{4}$$

For the actual calculation of background XSs, the enhanced neutron-current method [7] is used. Using the total reaction rate and the flux representation based on equivalence theory, the background XSs for a heterogeneous system can be obtained as follows:

$$\sum_{t,f}(E)\phi_f(E) = \sum_{t,f}(E) \frac{\sum_{p,f} + g(C, a_B)\sum_e}{\sum_{t,f}(E) + g(C, a_B)\sum_e} \tag{5}$$

where $\Sigma_{t,f}$ (E) represents the total XSs of the fuel, $\Sigma_{p,f}$ represents the potential XSs of the fuel, Σ_e is the escape XSs, ϕ_f (E) represents the neutron flux in the fuel, $g(C,a_B)$ is the Dancoff factor, C is the Dancoff correction factor (1− the Dancoff factor), and a_B is the Bell factor.

Using the black-limit approximation, ($\Sigma_{t,f}(E) \to \infty$), Eq. (5) can be written as:

$$\lim_{\sum_{t,f} \to \infty} \sum_{t,f}(E)\phi_f(E) = N^r \sigma_p^r + N^r \left(\sigma_{o,f} + g(C, a_B) \sum_e \Big/ N^r \right) \tag{6}$$

where $\sigma_{o,f}$ is the background XS of the homogeneous mixture. The Bondarenko XSs for a heterogeneous system can be obtained as:

$$\sigma_o = \frac{1}{N^r} \lim_{\sum_{t,f} \to \infty} \sum_{t,f}(E)\phi_f(E) - \sigma_p^r \tag{7}$$

Hence, the Bondarenko XSs are obtained by performing a fixed-source calculation for the total reaction rate with very large total XSs. A fixed-source problem is formed such that

$$\Omega \cdot \nabla\phi + \sum_t \phi = \frac{1}{4\pi} \lambda \sum_p \tag{8}$$

where

$$\lambda \sum_p = \sum_i \lambda_i N_i \sigma_{p,i} \tag{9}$$

and λ_i is the Goldstein-Cohen factor for the i^{th} nuclide. Other variables are defined above.

In the construction of this fixed-source problem, the following rules are applied: (1) the total XS in the fuel region is assumed to be as large as 10^4 cm^{-1} and the total and absorption XSs are set to be the same by neglecting the scattering

XSs; (2) the source intensities in all regions are set to $\lambda\Sigma_p$ for the region; (3) the total XS in each region, except the fuel region, is set to $\lambda\Sigma_p$.

Flux is obtained from a fixed-source calculation by the MOC transport solver from nTRACER, and the reaction rate is used to obtain the Bondarenko XS, which will give the background XS for each resonant isotope. As the background XSs are directly evaluated from a fixed-source solution at high total XSs, they require neither the Bell factor nor the escape probability. As the background XS evaluation does not use the escape–probability relations, rational approximations are not needed.

2.3. *Resonance-interference method*

The resonance treatment in the resolved-energy range for the single-resonant nuclide is straightforward, however, when there is more than one resonance absorber in the mixture, the straightforward approach does not work. The XSs for resonant nuclides are different in mixture and isolated configurations [9,10]. The RIFs for a resonant nuclide can be defined as the ratio of the XSs in the mixture to the XSs in the isolated configuration. The group-dependent RIFs are defined as:

$$f_{x,g}^{i}=\frac{\sigma_{x,g}^{mix,i}}{\sigma_{x,g}^{iso,i}}=\frac{\int_{\Delta u\in g}\sigma_x^i(u)\varphi^{mix,i}(u)du\Big/\int_{\Delta u\in g}\varphi^{mix,i}(u)du}{\int_{\Delta u\in g}\sigma_x^i(u)\varphi^{iso,i}(u)du\Big/\int_{\Delta u\in g}\varphi^{iso,i}(u)du} \tag{10}$$

where $f_{x,g}^{i}$ represents the RIF for group g, nuclide i, and reaction type x; $\sigma_x^{mix,i}, \sigma_x^{iso,i}$ are the microscopic XSs for nuclide i in reaction x in the mixture and isolated configurations, respectively, $\sigma_x^i(u)$ represents pointwise XSs on a union-lethargy grid, and $\varphi^{mix,i}(u)$, $\varphi^{iso,i}(u)$ are the self-shielded flux of the mixture of resonant nuclides and the isolated resonant nuclide, respectively. The indices for nuclide i in group g are dropped for convenience, however, these are considered to be specific for a resonant nuclide and energy group.

The approximate expressions for the self-shielded fluxes in the mixture, as well as the isolated configuration, can be derived using the slowing-down equation. Using the IR approximation, the slowing-down equation can be written as:

$$\sum_t(u)\varphi(u)=\sum_i\left(\lambda_i\sum_{p,i}+(1-\lambda_i)\sum_{s,i}(u)\varphi(u)\right) \tag{11}$$

where $\Sigma_t(u)$ is the total XS, $\Sigma_{p,i}$ represents the potential XS for nuclide i, $\Sigma_{s,i}(u)$ represents the scattering XS for nuclide i, $\varphi(u)$ is the lethargy-dependent flux, andλ_i is the Goldstein-Cohen factor. The total XS can be written as:

$$\sum_t(u)=\sum_a^F(u)+\sum_s^F(u)+\sum_p^M \tag{12}$$

where $\sum_a^F(u)+\sum_s^F(u)$, and $\sum_p^M$ are the fuel-absorption XSs, fuel-scattering XSs, and moderator-potential XSs, respectively.

$$\sum_s^F(u)=\sum_s^{F,res}(u)+\sum_p^F \tag{13}$$

where F and M represent the fuel and moderator elements, and $\sum_s^{F,res}$ is the fuel-resonance scattering XS:

$$\sum_i\lambda\sum_{p,i}=\lambda_F\sum_p^F+\lambda_M\sum_p^M=\lambda\sum_p \tag{14}$$

where λ_F,λ_M are the Goldstein-Cohen factors for fuel and moderator nuclides, enabling the following equation to be obtained for flux:

$$\varphi(u)=\frac{\lambda\sum_p}{\sum_a^F(u)+\lambda_F\sum_s^{F,res}(u)+\lambda\sum_p} \tag{15}$$

or in the form of background XS:

$$\varphi(u)=\frac{\sigma_b}{\sigma_a^F(u)+\lambda_F\sigma_s^{F,res}(u)+\sigma_b} \tag{16}$$

where

$$\sigma_b=\frac{\lambda\sum_p}{N} \tag{17}$$

As λ_F<<1 for heavy nuclides, the second term in the denominator, i.e., $\lambda_F\sigma_s^{F,res}(u)$, can be neglected. Therefore, Eq. (16) can be written as:

$$\varphi(u)=\frac{\sigma_b}{\sigma_a^F(u)+\sigma_b} \tag{18}$$

Eq. (18) provides the self-shielded flux for the isolated-resonant isotope. For the resonant nuclide in the mixture of absorbers, by neglecting the resonance elastic-scattering term in Eq. (15), the self-shielded flux can be approximated as [6]:

$$\varphi(u)=\frac{\lambda\sum_p}{\sum_a^F(u)+\lambda\sum_p} \tag{19}$$

where $\sum_a^F(u)$ contains all resonant absorbers in the fuel.

Using Eqs. (18) and (19), Eq. (10) can be re-written as:

$$f_x=\frac{\int\frac{\sigma_x(u)}{\sum_{ax}(u)+\lambda\sum_p}du\Big/\int\frac{1}{\sum_{ax}(u)+\lambda\sum_p}du}{\int\frac{\sigma_x(u)}{\sigma_{ax}(u)+\sigma_b}du\Big/\int\frac{1}{\sigma_{ax}(u)+\sigma_b}du} \tag{20}$$

Using the pointwise XSs, the integrals in Eq. (20) can be calculated numerically by Simpson's rule. The group-dependent RIFs are obtained from Eq. (20) for the evaluation of effective XSs for the resonant nuclides in mixed absorbers. Now, to correct the XSs for nuclide i, group g, the RIFs are multiplied by the effective XSs generated for the isolated-resonance nuclide, as given below:

$$\hat{\sigma}_{x,g}^{i}=f_{x,g}^{i}\sigma_{x,g}^{i} \tag{21}$$

where $\hat{\sigma}_{x,g}^{i}$ is the corrected XS after the resonance-interference treatment for isotope i, group g, and reaction x, while $\sigma_{x,g}^{i}$ is the uncorrected XS.

2.4. *Temperature-feedback effect*

RIF is a function of temperature, as well as background XS. RIFs are generated at the multigroup level for a range of temperatures and once per burnup step. During the reactor operation, the temperature variation causes variation in XSs.

At each temperature variation, it is impractical to calculate RIFs from the XS table directly because of the large number of lethargy points. However, the interpolation of XSs for the specific temperature will increase the calculation burden. These problems are not addressed in the NRIM-based method. In this approach, the temperature-feedback effect is incorporated with the temperature dependency of RIFs. The temperature-dependent multigroup RIFs are obtained from the XS table and stored for future use. As the temperature of the system changes, the RIFs are interpolated for that temperature at the multigroup level. The linear interpolation scheme is utilized for this thermal-feedback effect, as it provides accurate results without extra computational burden.

2.5. *Resonance absorption and escape probability*

In RIF calculation, the spectrum is approximated by IR approximation, as given in Eq. (19). The flux is approximated from the absorption XSs of the mixture. Not all the neutrons survive after passing through the resonance peak, as some of them are absorbed into the resonance peak. Therefore, the number of post-peak neutrons will be less than the number of pre-peak neutrons. The approximated spectrum does not incorporate this post-peak decreasing effect, which can also be termed as the energy self-shielding effect. This is one of the reasons for large errors in the lower energy range.

To incorporate this effect, the resonance-escape probability of a neutron needs to be determined. The balance equation with hydrogen as the scatterer is as follows [12]:

$$\sum_t(E)\varphi(E) - \int_E^{\infty}\sum_s^H(E')\varphi(E')\frac{dE'}{E'} = s_o\chi(E) \tag{22}$$

where $\Sigma_s^H(E')$ is the scattering XS of ^{1}H, s_o is the slowing-down density, and $\chi(E)$ is the energy spectrum. Other variables have the same meanings as in previous sections. The neutron spectrum in an infinite medium for energies below the source can be derived as:

$$\varphi(E) = \frac{s_o}{E\sum_t(E)}\exp\left[-\int_E^{E_u}\frac{\sum_a(E')}{\sum_t(E')}\frac{dE'}{E'}\right] \tag{23}$$

The resonance non-escape probability, $\overline{p}(E)$, is defined as:

$$\overline{p}(E) = \frac{1}{s_o}\int_E^{E_u}\sum_a(E')\varphi(E')dE' \tag{24}$$

Incorporating Eq. (23) into Eq. (24) and simplifying leads to:

$$\overline{p}(E) = 1 - \exp\left[-\int_E^{E_u}\frac{\sum_a(E')}{\sum_t(E')}\frac{dE'}{E'}\right] \tag{25}$$

The resonance-escape probability, $p(E)$, is:

$$p(E) = 1 - \overline{p}(E) = \exp\left[-\int_E^{E_u}\frac{\sum_a(E')}{\sum_t(E')}\frac{dE'}{E'}\right] \tag{26}$$

The integrals in Eq. (26) can be numerically evaluated by Simpson's rule. The resulting resonance-escape probability can be utilized to correct the spectrum:

$$\varphi(E) = \varphi_o(E)p(E) \tag{27}$$

where $\varphi_o(E)$ is the loss-free spectrum and $\varphi(E)$ is the corrected spectrum. This method is only applied to the lower energy range because of the large errors in the RIFs, as well as the XSs in this range.

3. Results and discussion

The method was verified by comparing the RIFs, XSs, and k-eff for homogeneous problems at various temperatures and burnup conditions. The efficiency of the resonance-escape probability treatment was analyzed in detail, as well as the temperature dependency of the RIFs, and the proposed method was compared to the currently available method. To support the method, heterogeneous pin-cell benchmark problem (1A) was analyzed for XSs verification, as well as reactivity accuracy. A heterogeneous pin cell with burned fuel was also analyzed.

3.1. *Homogeneous problem*

The accuracy of the modified XST method was confirmed by comparing the k-eff, as well as XSs, with McCARD [13] results. A homogeneous UO_2 fuel with 5% ^{235}U was burned to 30 MWD/kg-HM and 69MWD/kg-HM, and only four resonant nuclides, ^{235}U, ^{238}U, ^{239}Pu, and ^{240}Pu, were chosen. The compositions are given in Table 1. For both cases, ^{1}H was taken, such that it provided the background XS for ^{238}U to be ~60 barns (a typical PWR value). These problems were solved in order to examine the accuracy of the resonance XSs for nTRACER against the MG XS tallied from the corresponding McCARD run. Comparisons were made between the conventional method, XST, and modified XST with McCARD. The k-eff comparisons for homogeneous configurations are shown in Table 2, showing that the reactivity difference between the conventional method and McCARD was quite large. The modified XST method showed good agreement with the reference values. Exact RIF shown in the Fig. 1 through 4 represents the RIF obtained from the slowing-down solutions. The proposed method is denoted by IR while the NRIM-based method is denoted by NRIM. The RIFs and XSs are plotted in the resonance energy range (from 4 eV to 9.118 keV, in the WIMS library). Fig. 1 shows the ^{235}U absorption RIF and its error with exact RIF, indicating a >1% improvement for the proposed method. Fig. 2 shows the ^{238}U absorption RIF and its error. The RIFs improved by 0.5% using the new approach. Large

Table 1 – Compositions for homogeneous cases.

Nuclide	Case 1 30 MWD/Kg-HM (300 K)	Case 2 69 MWD/Kg-HM (600 K)
^{235}U	3.19778×10^{-04}	1.21099×10^{-04}
^{238}U	1.21432×10^{-02}	1.16636×10^{-02}
^{239}Pu	1.23197×10^{-04}	1.72235×10^{-04}
^{240}Pu	2.55014×10^{-05}	5.17223×10^{-05}
^{1}H	3.51917×10^{-02}	3.51775×10^{-02}

Table 2 – The k-eff calculation for homogeneous configurations.

Configurations	Method	k-eff	Reactivity difference Δρ (pcm)
Case 1	McCARD	1.18669 (2)	–
	Conventional	1.18501	−119
	Modified XST	1.18615	−38
Case 2	McCARD	1.06319 (5)	–
	Conventional	1.06133	−165
	Modified XST	1.06210	−97

pcm, per cent mille; XST, cross-section table.
Values in parentheses show standard deviation of keff.

improvements were observed in ^{239}Pu and ^{240}Pu, as shown in Figs. 3 and 4, respectively. The absolute error in the lower energy group decreased from 8% to 1% for ^{239}Pu, which confirmed the accuracy of the new approach. The RIFs calculated with this new method showed good agreement. RIFs were improved in the modified XST method, which contributed to XS accuracy. The errors in the RIFs for ^{240}Pu were large, however, were still improved from the conventional method. To verify the temperature-feedback effect, the percentage errors for calculated RIFs at 450 K and 750 K, respectively, are shown in Figs. 5 and 6. This new feature interpolates RIFs for the system temperature and is validated for all temperatures. These interpolated RIFs are compared with the exact RIFs calculated at 450K and 750K. The exact RIFs were obtained from two slowing-down solutions for a resonant nuclide, one in a mixture of absorbers and the other in the isolated case. The RIFs showed good agreement at other temperatures.

The microscopic absorption XSs are plotted with reactivity errors for ^{235}U in Fig. 7. The legends in all figures are described

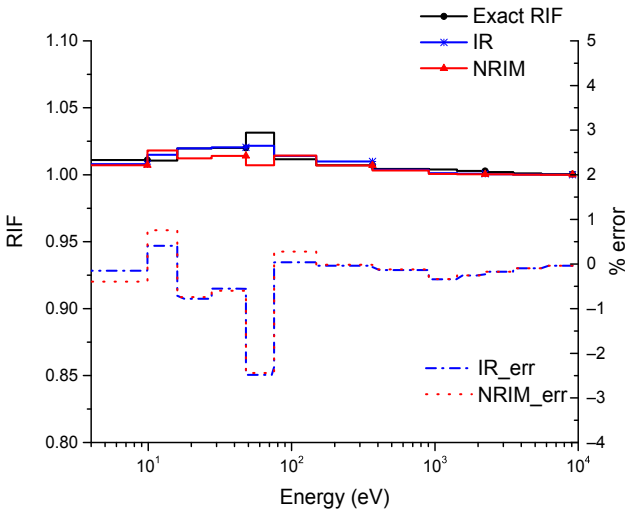

Fig. 2 – Comparison of absorption RIFs for ^{238}U. IR, intermediate resonance; IR_err, intermediate resonance error, NRIM, narrow resonance infinite mass; NRIM_err, narrow resonance infinite mass error; RIF, resonance-interference factor.

such that McCARD means values from McCARD calculations. Bondar means the results by the Bondarenko iteration method, XST means the XST without resonance escape probability treatment, and modified XST means the XST with resonance escape probability treatment. Furthermore, Bond_err means error for the Bondarenko iteration method, XST_err means error for the XSs table method, and modified XST err is the error for the modified XST method. Fig. 7 shows that the reactivity errors in the XSs were large for the conventional method, while the XSs showed good agreement

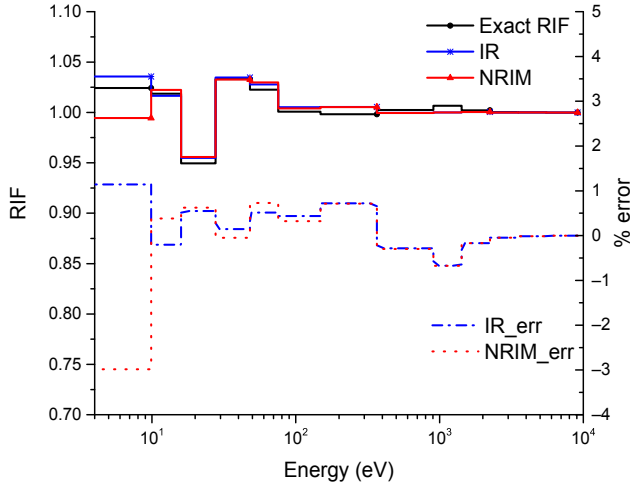

Fig. 1 – Comparison of absorption RIFs for ^{235}U. IR, intermediate resonance; IR_err, intermediate resonance error, NRIM, narrow resonance infinite mass; NRIM_err, narrow resonance infinite mass error; RIF, resonance-interference factor.

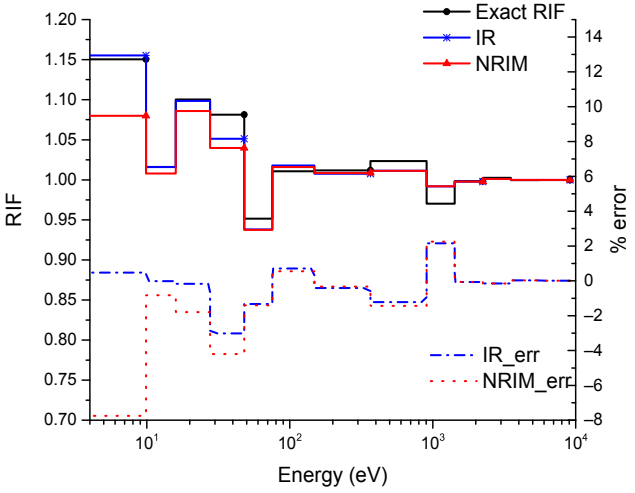

Fig. 3 – Comparison of absorption RIFs for ^{239}Pu. IR, intermediate resonance; IR_err, intermediate resonance error, NRIM, narrow resonance infinite mass; NRIM_err, narrow resonance infinite mass error; RIF, resonance-interference factor.

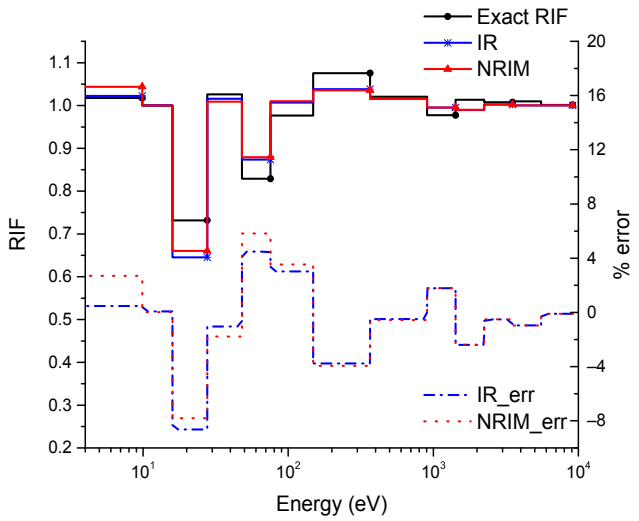

Fig. 4 – Comparison of absorption RIFs for ^{240}Pu. IR, intermediate resonance; IR_err, intermediate resonance error, NRIM, narrow resonance infinite mass; NRIM_err, narrow resonance infinite mass error; RIF, resonance-interference factor.

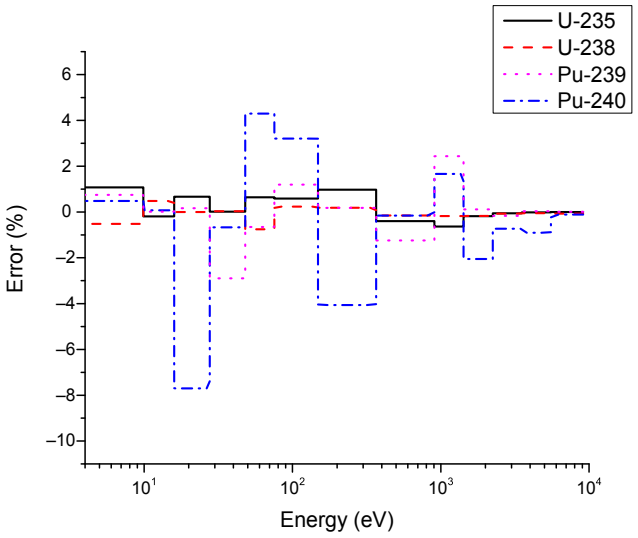

Fig. 6 – Comparison of absorption RIFs at 750 K. RIF, resonance-interference factor.

using the XST method, except in the lower energy range. Therefore, the modified XST provided good results at all energies. The fission XSs and the reactivity errors for ^{235}U are shown in Fig. 8. It is clear from the figure that the XSs improved considerably and that the error decreased significantly using XST and compared to the conventional method. A significant error reduction was also observed using modified XST. Fig. 9 shows the microscopic absorption XSs for ^{238}U. Although the errors in XSs using the modified XST were not significantly improved, the errors were still very small. For the microscopic absorption XSs of ^{239}Pu (Fig. 10), the errors in the XSs were significantly reduced by using the XST method. The error in the lower energy group was large, however, still smaller than that observed with the conventional method. The large error at lower energy was removed by using the modified XST method. The same trend was observed in the microscopic-fission XSs for ^{239}Pu (Fig. 11), indicating that the XSs obtained with the modified XST method were in agreement with McCARD-calculated XSs. The errors in the

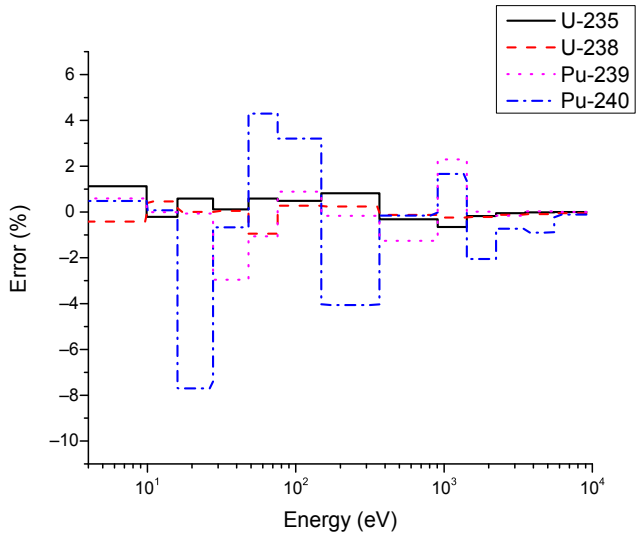

Fig. 5 – Comparison of absorption RIFs at 450 K. RIF, resonance-interference factor.

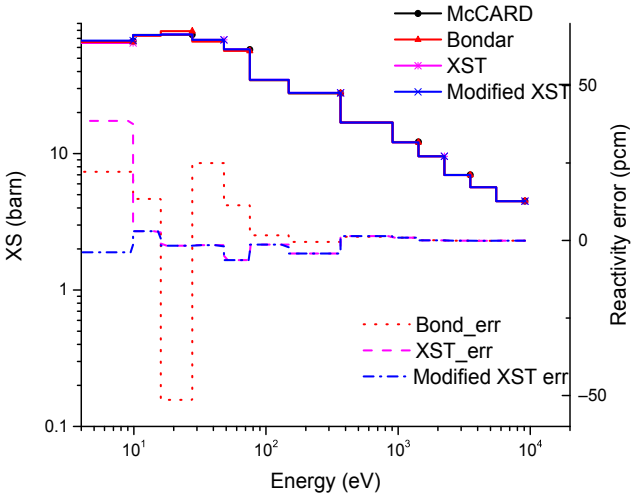

Fig. 7 – Microscopic absorption XSs and reactivity errors for ^{235}U (Case 1). Bondar, results by the Bondarenko iteration method; Bond_err, error for the Bondarenko iteration method; Modified XST, the cross-section table method with resonance-escape probability treatment; Modified XST_err, error for the modified XST method; pcm, per cent mille; XS, cross section; XST, cross-section table method without resonance-escape probability treatment; XST_err, error for the XST method.

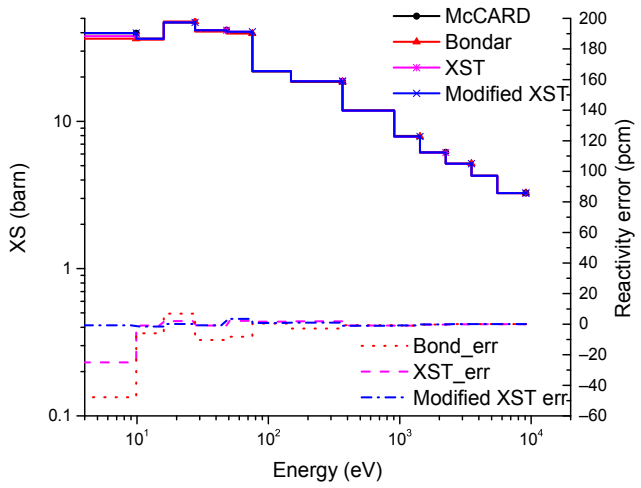

Fig. 8 – Microscopic fission XSs and reactivity errors for ^{235}U (Case 1). Bondar, results by the Bondarenko iteration method; Bond_err, error for the Bondarenko iteration method; Modified XST, the cross-section table method with resonance-escape probability treatment; Modified XST_err, error for the modified XST method; pcm, per cent mille; XS, cross section; XST, cross-section table method without resonance-escape probability treatment; XST_err, error for the XST method.

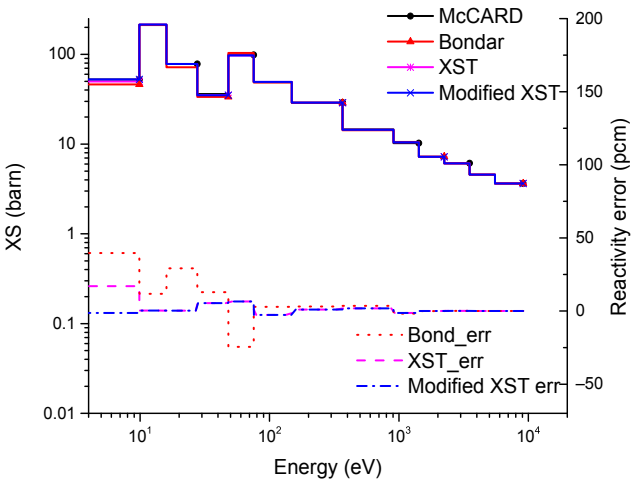

Fig. 10 – Microscopic absorption XSs and reactivity errors for ^{239}Pu (Case 1). Bondar, results by the Bondarenko iteration method; Bond_err, error for the Bondarenko iteration method; Modified XST, the cross-section table method with resonance-escape probability treatment; Modified XST_err, error for the modified XST method; pcm, per cent mille; XS, cross section; XST, cross-section table method without resonance-escape probability treatment; XST_err, error for the XST method.

absorption XSs for ^{240}Pu (Fig. 12) were large, but still smaller than those observed in the conventional method. To check the applicability of the method at various temperatures and burnups, case two was analyzed with a different enrichment, burnup, and temperature. The temperature was 600 K and the burnup was 69 MWD/kg-HM. Figs. 13 and 14 show the absorption and fission XSs for ^{235}U, respectively. The XSs exhibited the same trend as in case one and showed good agreement. Fig. 15 shows the absorption XSs for ^{238}U, indicating good results for the modified XST method. Figs. 16 and

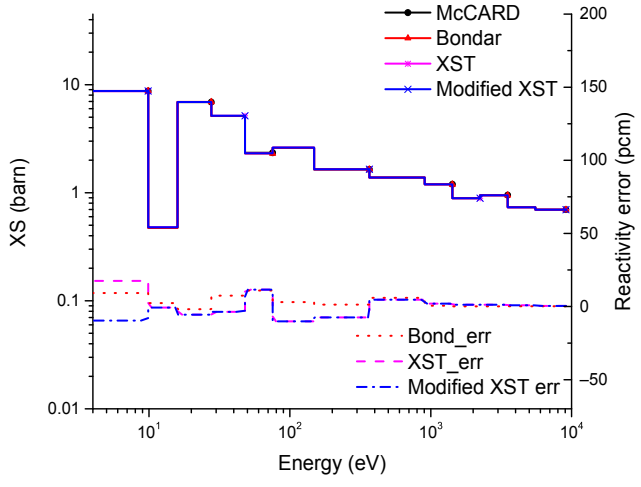

Fig. 9 – Microscopic absorption XSs and reactivity errors for ^{238}U (Case 1). Bondar, results by the Bondarenko iteration method; Bond_err, error for the Bondarenko iteration method; Modified XST, the cross-section table method with resonance-escape probability treatment; Modified XST_err, error for the modified XST method; pcm, per cent mille; XS, cross section; XST, cross-section table method without resonance-escape probability treatment; XST_err, error for the XST method.

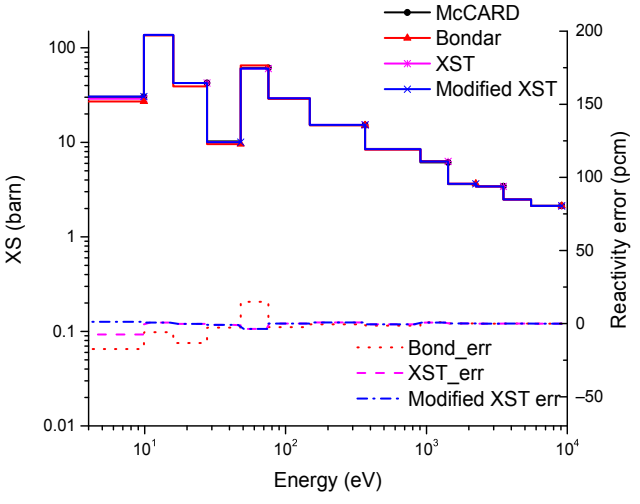

Fig. 11 – Microscopic fission XSs and reactivity errors for ^{239}Pu (Case 1). Bondar, results by the Bondarenko iteration method; Bond_err, error for the Bondarenko iteration method; Modified XST, the cross-section table method with resonance-escape probability treatment; Modified XST_err, error for the modified XST method; pcm, per cent mille; XS, cross section; XST, cross-section table method without resonance-escape probability treatment; XST_err, error for the XST method.

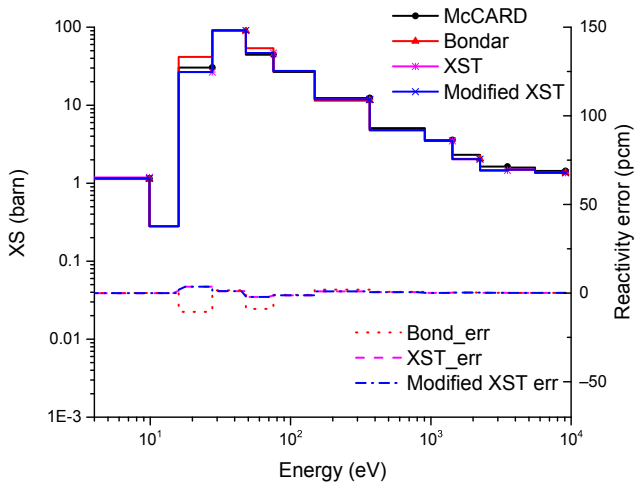

Fig. 12 – Microscopic absorption XSs and reactivity errors for ^{240}Pu (Case 1). Bondar, results by the Bondarenko iteration method; Bond_err, error for the Bondarenko iteration method; Modified XST, the cross-section table method with resonance-escape probability treatment; Modified XST_err, error for the modified XST method; pcm, per cent mille; XS, cross section; XST, cross-section table method without resonance-escape probability treatment; XST_err, error for the XST method.

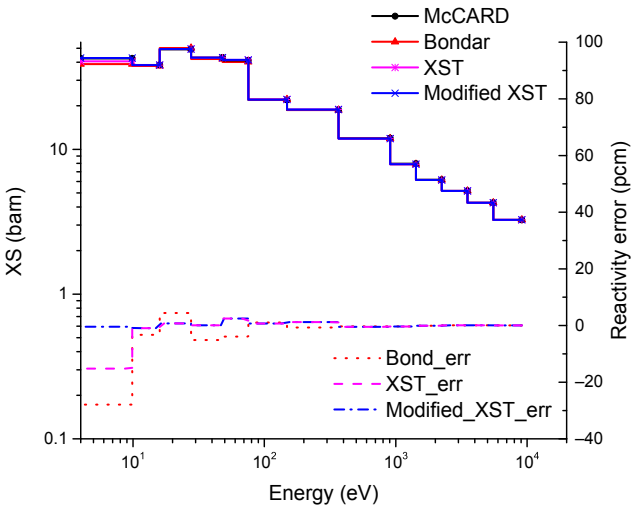

Fig. 14 – Microscopic fission XSs and reactivity errors for ^{235}U (Case 2). Bondar, results by the Bondarenko iteration method; Bond_err, error for the Bondarenko iteration method; Modified XST, the cross-section table method with resonance-escape probability treatment; Modified XST_err, error for the modified XST method; pcm, per cent mille; XS, cross section; XST, cross-section table method without resonance-escape probability treatment; XST_err, error for the XST method.

17 show the absorption XSs for ^{239}Pu and ^{240}Pu, respectively, and show large errors from the conventional method. For the XST method, the errors were reduced noticeably, however, large errors remained at the lower energy range. These errors were eliminated by using the modified XST method. Based on these XSs data, the proposed method worked well for the homogeneous configuration for any enrichment, composition, temperature, and burnup. Also, the method efficiently incorporated the temperature-feedback effect for RIFs.

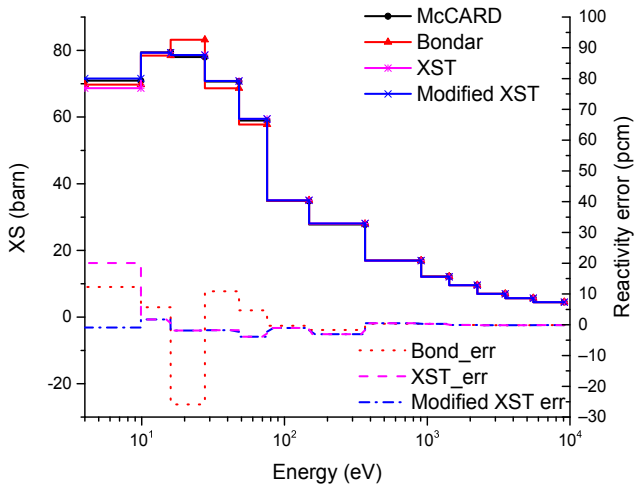

Fig. 13 – Microscopic absorption XSs and reactivity errors for ^{235}U (Case 2). Bondar, results by the Bondarenko iteration method; Bond_err, error for the Bondarenko iteration method; Modified XST, the cross-section table method with resonance-escape probability treatment; Modified XST_err, error for the modified XST method; pcm, per cent mille; XS, cross section; XST, cross-section table method without resonance-escape probability treatment; XST_err, error for the XST method.

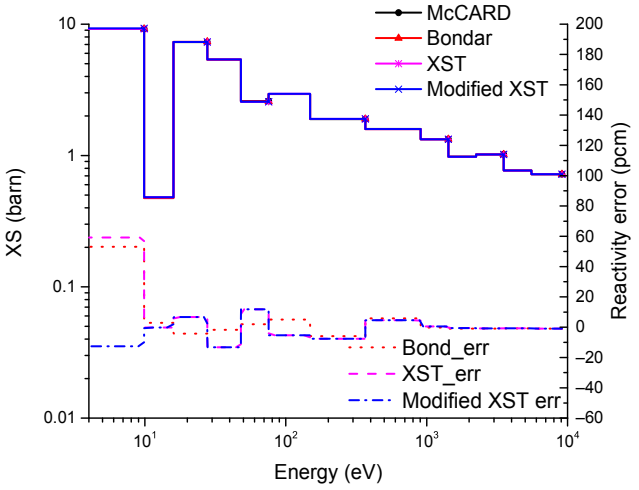

Fig. 15 – Microscopic absorption XSs and reactivity errors for ^{238}U (Case 2). Bondar, results by the Bondarenko iteration method; Bond_err, error for the Bondarenko iteration method; Modified XST, the cross-section table method with resonance-escape probability treatment; Modified XST_err, error for the modified XST method; pcm, per cent mille; XS, cross section; XST, cross-section table method without resonance-escape probability treatment; XST_err, error for the XST method.

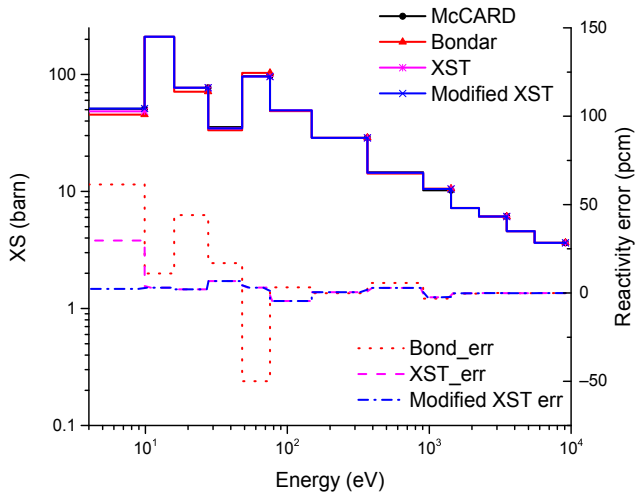

Fig. 16 – Microscopic absorption XSs and reactivity errors for ^{239}Pu (Case 2).Bondar, results by the Bondarenko iteration method; Bond_err, error for the Bondarenko iteration method; Modified XST, the cross-section table method with resonance-escape probability treatment; Modified XST_err, error for the modified XST method; pcm, per cent mille; XS, cross section; XST, cross-section table method without resonance-escape probability treatment; XST_err, error for the XST method.

3.2. *Heterogeneous problems*

After verification of the method for the homogeneous configurations, two heterogeneous problems were analyzed at different burnup conditions.

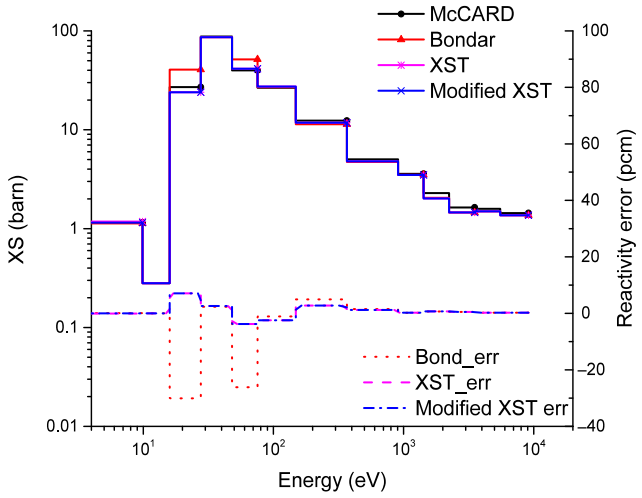

Fig. 17 – Microscopic absorption XSs and reactivity errors for ^{240}Pu (Case 2). Bondar, results by the Bondarenko iteration method; Bond_err, error for the Bondarenko iteration method; Modified XST, the cross-section table method with resonance-escape probability treatment; Modified XST_err, error for the modified XST method; pcm, per cent mille; XS, cross section; XST, cross-section table method without resonance-escape probability treatment; XST_err, error for the XST method.

3.3. *VERA pin-cell benchmark problem*

VERAs represent the Consortium for Advanced Simulation of Light-water reactors core physics benchmark problems [14]. For the XS comparison in the benchmark configuration, the heterogeneous pin cell (1A) was selected. The composition and geometry are given in Table 3 and Fig. 18, respectively, and nuclide concentrations in the fuel are given in Table 4. Fig. 19 shows the absorption XSs for ^{235}U, with reactivity errors for both methods. Modified XST showed good results as compared to the conventional method. Fig. 20 shows the fission XSs for ^{235}U. Figs. 18–20 show that the errors in the XSs were significantly reduced and that the XSs were improved for ^{238}U as compared to the conventional method (Fig. 21). Table 5 shows the reactivity comparison for various VERA pin-cell problems using various methods. The term nTRACER_conv represents the conventional method in nTRACER. This problem will be denoted by 1A. The reactivity difference for modified XST was <182 pcm, which was larger than the conventional method, but in the latter case, the lesser error may be due to error cancellation. In Figs. 7, 10, 13 and 16, the conventional method exhibited both positive and negative reactivity errors, resulting in error cancellation. The XS error was reduced noticeably using the modified XST method. The heterogeneous pin-cell problem confirmed the accuracy of the method.

Table 3 – Composition and geometry of VERA pin cell.

Geometry	Radius (cm)	Composition	Density (g/cm^3)	Temp (K)
Fuel	0.4096	UO_2	10.257	565
Gap	0.418	Air	–	
Cladding	0.475	Zr-4	–	
Moderator	–	H_2O	0.743	
Pitch	1.26	–	–	–

VERA, virtual environment for reactor application.

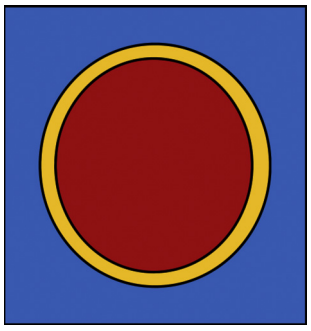

Fig. 18 – Pin-cell geometry.

Table 4 – Fuel-pellet composition.

Nuclide	Weight (%)
^{234}U	0.0263
^{235}U	3.1
^{236}U	0.0143
^{238}U	96.8594

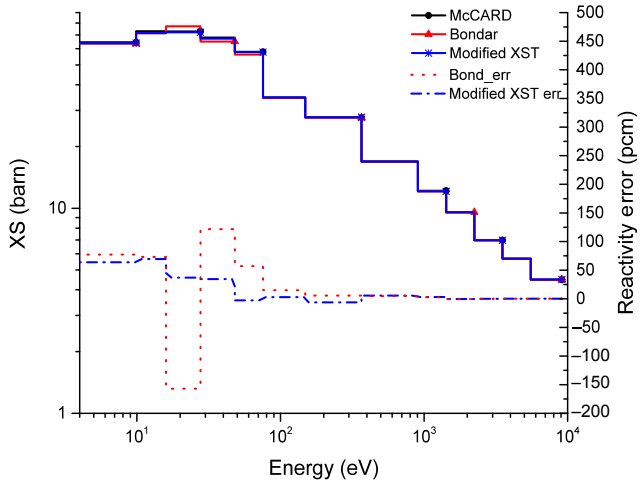

Fig. 19 – Microscopic absorption XSs and reactivity errors for ^{235}U (1A). Bondar, results by the Bondarenko iteration method; Bond_err, error for the Bondarenko iteration method; Modified XST, the cross-section table method with resonance-escape probability treatment; Modified XST_err, error for the modified XST method; pcm, per cent mille; XS, cross section.

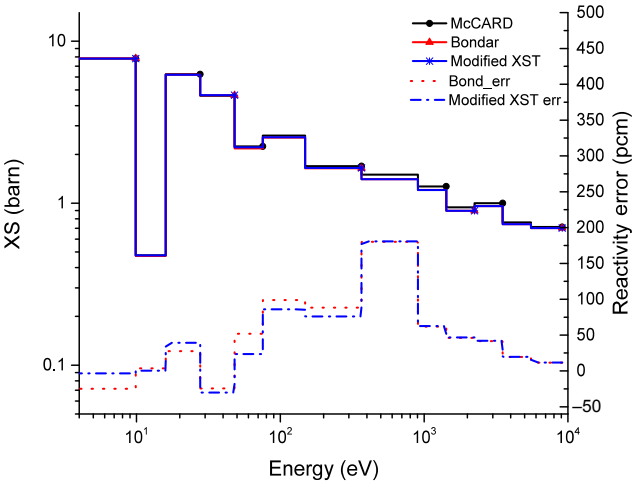

Fig. 21 – Microscopic absorption XSs and reactivity errors for ^{238}U (1A). Bondar, results by the Bondarenko iteration method; Bond_err, error for the Bondarenko iteration method; Modified XST, the cross-section table method with resonance-escape probability treatment; Modified XST_err, error for the modified XST method; pcm, per cent mille; XS, cross section.

3.4. *Heterogeneous pin cell*

A heterogeneous pin cell was considered with the same geometry and composition as the VERA pin cell shown in Fig. 18 and Table 3. This problem was denoted by a burned case. The compositions for four selected resonant nuclides were obtained from 5% enriched UO_2 fuel at 30MWD/Kg-HM. The number densities for ^{235}U, ^{238}U, ^{239}Pu, and ^{240}Pu were 3.94226×10^{-4}, 2.12946×10^{-2}, 1.90362×10^{-4}, and 1.84419×10^{-5} #/barn-cm, respectively. The calculations were performed at 600 K. The k-eff and XSs obtained using the modified XST and conventional methods were compared with McCARD values. In Table 6, the k-eff for the problem is given based on the above-mentioned methods. The reactivity difference for the conventional method was large, while the reactivity improved using the modified XST method. Figs. 22 and 23 show the microscopic absorption and fission XSs for ^{235}U, respectively. The XSs improved considerably using the

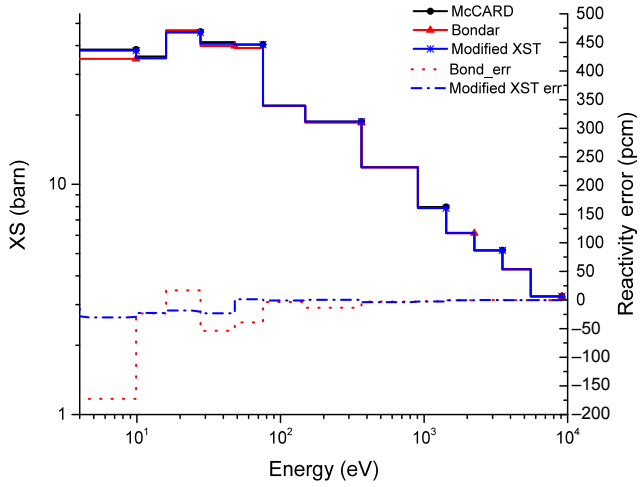

Fig. 20 – Microscopic fission XSs and reactivity errors for ^{235}U (1A). Bondar, results by the Bondarenko iteration method; Bond_err, error for the Bondarenko iteration method; Modified XST, the cross-section table method with resonance-escape probability treatment; Modified XST_err, error for the modified XST method; pcm, per cent mille; XS, cross section.

Table 5 – The k-eff comparison for various methods.

Case	Condition	Method	k-eff	Δρ (pcm) Diff., pcm
1A	565 K	KENO-VI	1.18704 (8)	–
	0.743 g/cc	nTRACER_nTL	1.18654	−35
		nTRACER_conv	1.18821	83
		nTRACER_WIL	1.18938	166
		McCARD	1.18762 (6)	41
1B	600 K	KENO-VI	1.18215 (8)	–
	0.661 g/cc	nTRACER_nTL	1.18211	−3
		nTRACER_conv	1.18379	117
		nTRACER_WIL	1.18470	182
		McCARD	1.18244 (7)	21
1C	900 K	KENO-VI	1.17172 (8)	–
	0.661 g/cc	nTRACER_nTL	1.17127	−33
		nTRACER_conv	1.17275	75
		nTRACER_WIL	1.17358	135
		McCARD	1.17241 (6)	50
1D	1,200 K	KENO-VI	1.16260 (8)	–
	0.661 g/cc	nTRACER_nTL	1.16208	−39
		nTRACER_conv	1.16263	2
		nTRACER_WIL	1.16408	109
		McCARD	1.16374 (6)	84

nTL, nTRACER library; pcm, per cent mille; WIL, WIMS library. Values in parentheses show the standard deviation in keff.

Table 6 – The k-eff calculation for heterogeneous burned case.

Configuration	Method	k-eff	Reactivity difference (pcm) Δρ (pcm)
Case 1	McCARD	1.33437 (6)	–
	Conventional	1.32547	−503
	Modified XST	1.32945	−277

pcm, per cent mille; XST, cross-section table.
Values in parentheses show the standard deviation in keff.

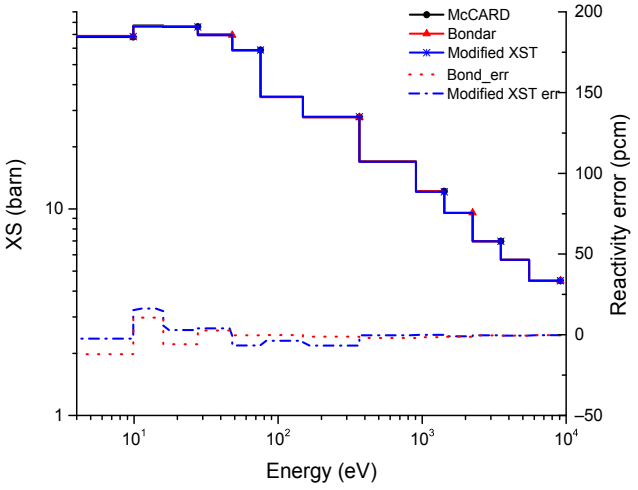

Fig. 22 – Microscopic absorption XSs and reactivity errors for ^{235}U (burned case). Bondar, results by the Bondarenko iteration method; Bond_err, error for the Bondarenko iteration method; Modified XST, the cross-section table method with resonance-escape probability treatment; Modified XST_err, error for the modified XST method; pcm, per cent mille; XS, cross section.

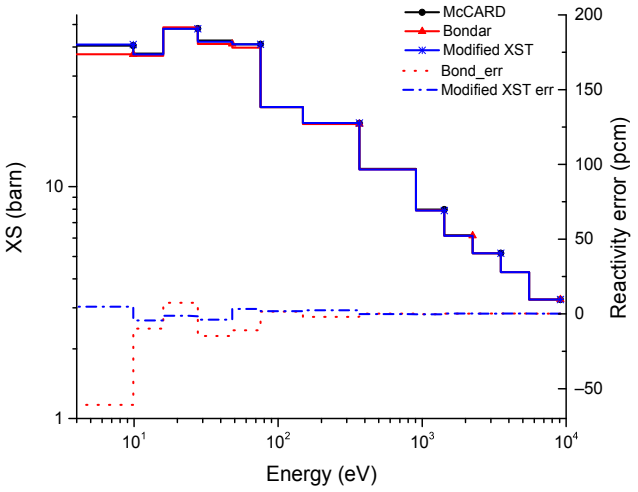

Fig. 23 – Microscopic fission XSs and reactivity errors for ^{235}U (burned case).Bondar, results by the Bondarenko iteration method; Bond_err, error for the Bondarenko iteration method; Modified XST, the cross-section table method with resonance-escape probability treatment; Modified XST_err, error for the modified XST method; pcm, per cent mille; XS, cross section.

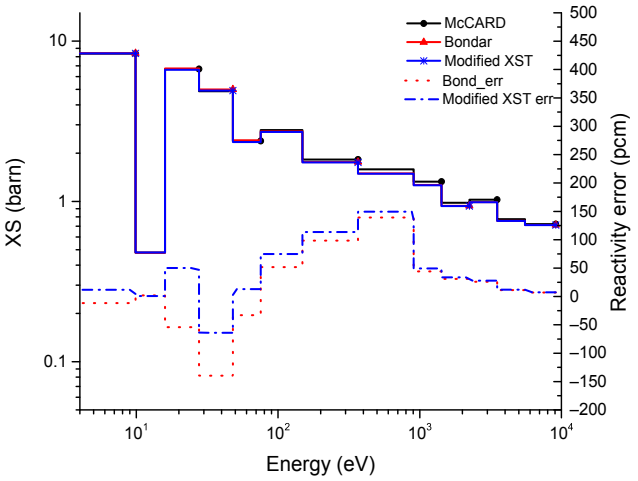

Fig. 24 – Microscopic absorption XSs and reactivity errors for ^{238}U (burned case). Bondar, results by the Bondarenko iteration method; Bond_err, error for the Bondarenko iteration method; Modified XST, the cross-section table method with resonance-escape probability treatment; Modified XST_err, error for the modified XST method; pcm, per cent mille; XS, cross section.

modified XST method. For ^{238}U-absorption XSs (Fig. 24), there was competition between the conventional and modified XST methods. Overall, the errors were reduced using the modified XST method. Figs. 25 and 26 show the absorption XSs for ^{239}Pu and ^{240}Pu, respectively, which were improved using the modified XST method.

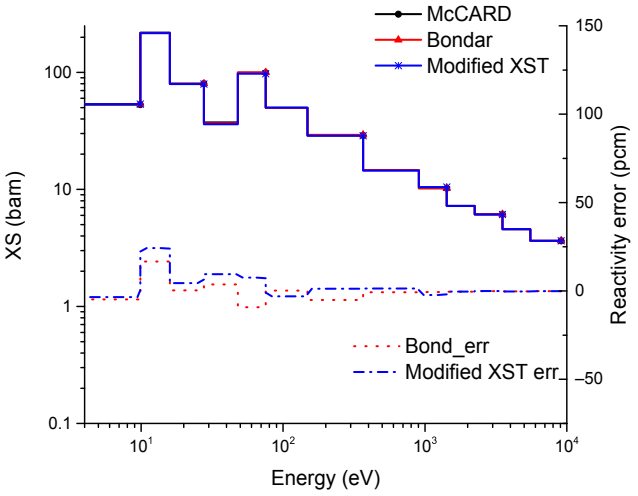

Fig. 25 – Microscopic absorption XSs and reactivity errors for ^{239}Pu (burned case). Bondar, results by the Bondarenko iteration method; Bond_err, error for the Bondarenko iteration method; Modified XST, the cross-section table method with resonance-escape probability treatment; Modified XST_err, error for the modified XST method; pcm, per cent mille; XS, cross section.

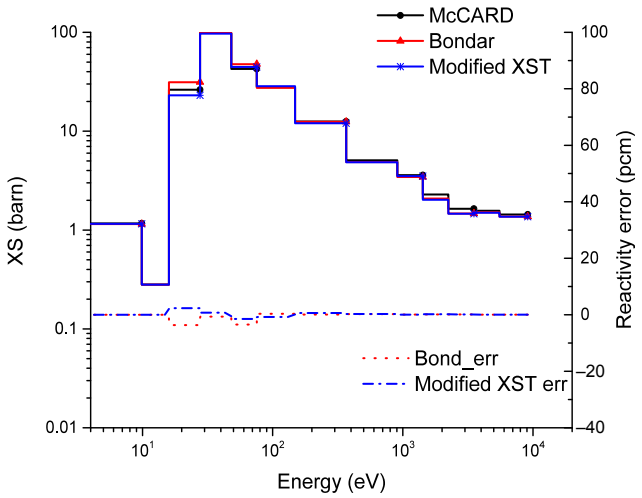

Fig. 26 – Microscopic absorption XSs and reactivity errors for ^{240}Pu (burned case). Bondar, results by the Bondarenko iteration method; Bond_err, error for the Bondarenko iteration method; Modified XST, the cross-section table method with resonance-escape probability treatment; Modified XST_err, error for the modified XST method; pcm, per cent mille; XS, cross section.

4. Conclusion

A resonance interference-treatment method based on the microscopic XS table with IR approximation was implemented in nTRACER. This method was modified from the NRIM or WR approximation to the IR approximation and the resonance elastic-scattering term was neglected. Another modification was the incorporation of resonance-escape probability to correct the spectrum. These modifications improved RIFs by 1% in uranium isotopes and 7% in plutonium isotopes, and improved the XSs relative to the NRIM-based method. The RIF comparison of both methods verified that the results were improved by using IR approximation with the resonance-escape probability, which contributed greatly to XS accuracy. The modified XST provided good agreement with the reference values for the homogeneous and heterogeneous pin-cell configurations. The proposed method allowed better results than the conventional method and reduced errors noticeably. The reactivity estimation of the modified XST method for the homogeneous configuration was good, while the conventional method resulted in large errors in both cases. The error in XSs was small in the case of the modified XST method, which also accurately predicted the XSs. The error in the absorption XSs for ^{238}U was large using the modified XST, but still smaller than that observed in the conventional method. The errors in ^{239}Pu and ^{240}Pu were also smaller than the conventional method. A new feature that incorporates the temperature-feedback effect of the RIFs showed good interpolation results. The RIFs were able to be calculated at the multigroup level for temperature variation within a very short time. With this feature, nTRACER accurately predicted the XSs by incorporating the resonance interference for mixed absorbers. This method also efficiently calculated RIFs at system temperatures other than those provided by the library. This method required RIF evaluation only once per burnup and did not require table search. These results indicate that the method was more efficient than the RIF table method. The accuracy was improved with the application of resonance-escape probability and better than that observed in the conventional method. This method is applicable for various configurations and rapid temperature variations.

Conflicts of interest

The authors have no conflict of interest.

Acknowledgments

This work was supported by the Ministry of Science, ICT and Future Planning of Korea through National Research Foundation of Korea under Grant No. NRF-2014M2A8A2074094.

REFERENCES

[1] R.J.J. Stamm'ler, M.J. Abbate, Methods of Steady-state Reactor Physics in Nuclear Design, Academic Press, London, 1983.
[2] D.G. Cacuci, Handbook of Nuclear Engineering, Springer, Berlin, 2010.
[3] H.G. Joo, G.Y. Kim, L. Pogosbekyan, Subgroup weight generation based on shielded pin-cell cross section conservation, Ann. Nucl. Energy 36 (2009) 859–868.
[4] Y.S. Jung, C.B. Shim, C.H. Lim, H.G. Joo, Practical numerical reactor employing direct whole core neutron transport and sub-channel thermal/hydraulic solvers, Ann. Nucl. Energy 62 (2013) 357–374.
[5] M.B. Chadwick, et al., ENDF/B-VII.0: next generation evaluated nuclear data library for Nuclear Science and Technology, Nucl. Data Sheets 107 (2006) 2931–3060.
[6] F. Leszczynski, D. Lopez Aldama, A. Trkov, WIMS Library Update, IAEA, Vienna, 2007.
[7] A. Yamamoto, Evaluation of background cross sections for heterogeneous and complicated geometry by the enhanced neutron current method, J. Nucl. Sci. Technol. 45 (2008) 1287–1292.
[8] Z. Gao, Y. Xu, T.J. Downar, The treatment of resonance interference effects in the subgroup method, Ann. Nucl. Energy 38 (2011) 995–1103.
[9] S. Choi, A. Khassenov, D.J. Lee, Resonance self-shielding method with resonance interference factor library, Trans. Am. Nucl. Soc. (Abstract) California (2014).
[10] M.L. Williams, Correction of multigroup cross sections for resolved resonance interference in mixed absorbers, Nucl. Sci. Eng. 83 (1983), 73–49.
[11] R.E. MacFarlane, et al., The NJOY Nuclear Data Processing System, Ver. 2012, Los Alamos National Laboratory, New Mexico, 2012.
[12] K.O. Ott, W.A. Bezella, Introductory Nuclear Reactor Statics, American Nuclear Society, 555 North Kensington Avenue, La Grange Park, Illinois, USA, 1989.
[13] H.J. Shim, B.S. Han, J.S. Jung, H.J. Park, C.H. Kim, McCARD: Monte Carlo code for advanced reactor design and analysis, Nucl. Eng. Technol. 44 (2012) 161–176.
[14] A.T. Godfrey, VERA Core Physics Benchmark Progression Problem Specifications, CASL-U-2012-0131-003, 2014.